ACS OMEGA

http://pubs.acs.org/journal/acsodf

Article

Synthesis of Silver(I) Complexes Containing 3-Oxo-3-phenyl-2-(2-phenylhydrazono)propanal-Based Ligands as a Multifunction Platform for Antimicrobial and Optoelectronic Applications

Ahlam I. Al-Sulami,* Maram T. Basha, Huda A. AlGhamdi, Sarah S. Albalawi, Khadijah M. Al-Zaydi, and Musa A. Said*

Cite This: *ACS Omega* 2023, 8, 23633−23642

Read Online

ACCESS | Metrics & More | Article Recommendations | Supporting Information

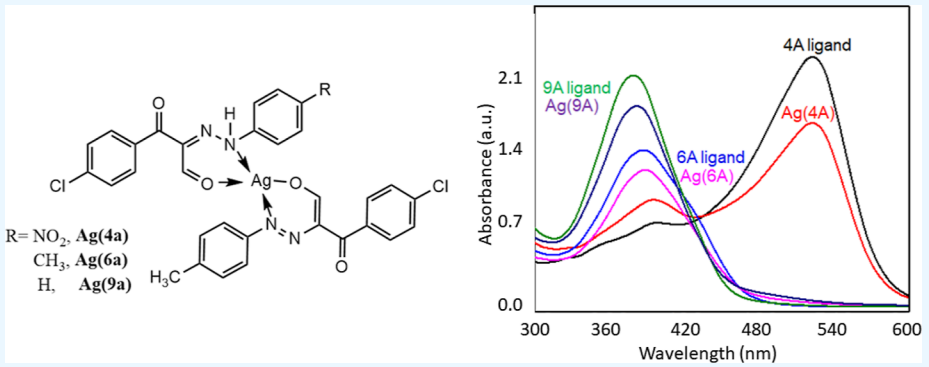

ABSTRACT: Toward multifunctionality, including antimicrobial and optoelectronic applications, herein, we reported the synthesis of a novel Ag(I) complex with 3-oxo-3-phenyl-2-(2-phenylhydrazono)propanal-based ligands including 3-(4-chlorophenyl)-2-[2-(4-nitrophenyl)hydrazono]-3-oxopropanal (named as "**4A**"), 3-(4-chlorophenyl)-2-[2-(4-methylphenyl)hydrazono]-3-oxopropanal (named as "**6A**"), and 3-(4-chlorophenyl)-3-oxo-2-(2-phenylhydrazono)propanal (named as "**9A**"). The synthesized compounds were characterized through FTIR, ^{1}H NMR, and density functional theory (DFT). The morphological features and thermal stability were evaluated through transmission electron microscopy (TEM) and TG/DTA analysis. The antimicrobial activity of the synthesized Ag complexes was tested against various pathogens, including Gram-negative bacteria (*Escherichia coli* and *Klebsiella pneumonia*), Gram-positive bacteria (*Staphylococcus aureus* and *Streptococcus mutans*), and fungi (*Candida albicans* and *Aspergillus niger*). Results show that the synthesized complexes (Ag(**4A**), Ag(**6A**), and Ag(**9A**)) possess promising antimicrobial efficacy against various pathogens and are in good competition with several standard drugs as well. On the other hand, the optoelectronic features such as absorbance, band gap, and Urbach energy were examined by measuring the absorbance using a UV−vis spectrophotometer. The values of the band gap reflected the semiconducting nature of these complexes. The complexation with Ag resulted in a lowering band gap to match the apex of the solar spectrum. Such low band gap values are preferable for optoelectronic applications like dye-sensitized solar cells, photodiodes, and photocatalysis.

1. INTRODUCTION

The increasing resistance of microorganisms to antimicrobial drugs is of global concern because of posing severe threat to public health worldwide.[1] Antimicrobial resistance affects human's ability to reduce the risk of infections caused by viruses, bacteria, fungi, and parasites.[2] The most common and threatening infections caused by multidrug-resistant microorganisms include the urinary tract, bloodstream, skin, soft tissue, osteoarticular, heart, and lung valve infections.[3] The most common antibacterial resistance pathogens, including *Staphylococcus aureus*, *Enterococcus faecium*, *Klebsiella pneumonia*, *Pseudomonas aeruginosa*, *Acetinobacter baumanii*, and *Enterobacteriaceae*, pose a severe threat worldwide because of the leading cause of nosocomial infections.[4,5,5] Moreover, fungal infections (candidiasis) need to be addressed to reduce the risk of their infections.[6] Generally, antimicrobial resistance generates because of genetic mutations of microorganisms toward excessive and rapid exposure to antimicrobial drugs.[7] As a result of mutation, several antimicrobial drugs such as cephalosporin, penicillins, quinolones, macrolides, vancomycin, methicillin, imipenem, ceftriaxone, co-trimoxazole, sulfona-

Received: March 10, 2023
Accepted: May 25, 2023
Published: June 7, 2023

ACS Publications

© 2023 The Authors. Published by American Chemical Society

mides, tetracycline, aminoglycosides, and chloramphenicol are becoming ineffective against several microbial strains.[8,9] Thus, the need to develop new and efficient antimicrobial drugs is rising to replace the commercially available drugs with poor antimicrobial efficacy.

Silver (Ag) has been widely used as an antimicrobial agent because of its strong toxicity against microorganisms.[10,11] Interestingly, Ag shows strong antimicrobial activity in an ionic or complexed state; however, it shows no antimicrobial activity in elemental form "nanocrystalline".[12] Initially, Ag^+ was widely applied in medical ointments, coating materials, or as an additive in drinking water for disinfection. However, the usage of Ag^+ decreased as it was quickly reduced to metallic Ag^0 in the skin from the action of the reducing agent.[13] Thus, the synthesis of Ag-containing complexes has attracted great interest because of the advantages of high stability and strong antimicrobial properties. The antimicrobial activity of Ag and its complexes could be attributed to the ionized form of Ag^+ that exhibits a strong association with substances such as nitrogen, sulfur, and oxygen, thus depriving bacteria from growth and even respiration.[14] Thus, Ag complexes have been widely applied in the medicinal and pharmaceutical industries because of their antimicrobial and anticancer features.[15] Additionally, these organometallic or Ag complexes may offer the opportunity to develop or even discover new active antimicrobial species based on their virtually infinite design options and three-dimensional geometry, offering a wide range of substitution options to target biomolecules.[16,17]

Recently, it has been observed that complexes of Ag(I) with some ligands containing N/O donor atoms exhibit a broad spectrum of antimicrobial properties because of strong interaction with bacteria.[18] Briefly, the antimicrobial properties of these compounds can be explained through chelation theory.[19] According to this theory, the overlap of metal and ligand orbitals leads to a decrease in the polarity of the metal ions, thus resulting in partial sharing of the metal ions with the donor group. Many complexes such as the Ag(I) complex with *N*-acetyl-L-cysteine and amino acids glycine, aspartic acid, and asparagine have shown promising antimicrobial efficacy against both Gram-negative and Gram-positive bacteria and even against yeast.[20] Recently, the β-diketone class of organic compounds and their copper complexes have attracted great interest because of tremendous pharmacological, antitumor, antiviral, and antioxidant activities.[21−24] Despite the fact that a wide range of these complexes have been synthesized to date, there is an urgent need to explore novel N/O donor ligands with strong ability to fight against drug-resistant pathogens.

Similarly, in solar cells, the commercially available Spiro-OMeTAD has been extensively applied as a hole transport material (HTM) because it fulfilled the highest effect solar cell ∼25.2%. However, complicated preparation of Spiro-OMeTAD alongside its high cost hinders its large-scale commercialization.[24] Therefore, extensive efforts have been made to find such alternatives that could replace Spiro-OMeTAD. To meet this demand, most of HTMs need dopants to boost their mobility and conductivity to achieve high efficiency.[24] Unfortunately, these dopants deteriorate the solar cell *via* the hygroscopic nature and transfer of ions to the absorber layer.[25] Based on these limitations, the demand for the development of dopant-free HTMs is of urgent need in the photovoltaic community.

Thus, keeping in view the above-mentioned future needs, herein we have successfully synthesized novel Ag(I) complexes with 3-oxo-3-phenyl-2-(2-phenylhydrazono)propanal-based ligands and evaluated their antimicrobial activity toward drug-resistant pathogens and optical properties. A series of Ag(I) complexes coordinating 3-(4-chlorophenyl)-2-[2-(4-nitrophenyl)hydrazono]-3-oxopropanal (named as "**4A**"), 3-(4-chlorophenyl)-2-[2-(4-methylphenyl)hydrazono]-3-oxopropanal (named as "**6A**"), and 3-(4-chlorophenyl)-3-oxo-2-(2-phenylhydrazono)propanal (named as "**9A**") have been synthesized, and their potential antimicrobial activity was evaluated against various pathogens including Gram-negative bacteria (*Escherichia coli* and *K. pneumonia*), Gram-positive bacteria (*S. aureus* and *Streptococcus mutans*), and fungi (*Candida albicans* and *Aspergillus niger*).[26] Further, the optoelectronic application has been evaluated by investigating the optical properties and band gap energies of these complexes. The composition of the synthesized ligands and their Ag(I) complexes were analyzed through FTIR, UV−visible absorption spectra, and ^{1}H NMR. In contrast, the morphology and stability were evaluated through TEM and thermal decomposition analysis (TGA/DTA). Results suggest that the synthesized novel Ag(I) complexes show promising antimicrobial activity against drug-resistant pathogens, and their efficacy is in good competition with the standard drugs.

2. EXPERIMENTAL SECTION

2.1. Materials and Instrumentation. All chemicals were utilized without further purification. Analytical grade silver(I) nitrate, sodium nitrite, arylamine hydrochloride, enaminone, sodium acetate, methanol, and ethanol were purchased from Sigma-Aldrich.

The UV−visible absorption spectra of ligands and their synthesized complexes were recorded using a Shimadzu 1800 UV−vis spectrophotometer (Japan) equipped with personal spectroscopy software version 2.3. The infrared spectra (KBr) were recorded on a Perkin−Elmer model Frontier (USA), whereas the ^{1}H NMR (700 MHz) spectra were recorded by employing the Bruker DPX 400 MHz spectrometer using 10 mg of the sample and tetramethylsilane (TMS) as an internal standard. A Shimadzu TGA-50H thermal analyzer (Japan) was used to analyze thermogravimetric analysis (TGA) measurements. The measurements were performed over the temperature range of 25−600 °C at a constant heating rate of 10 °C/min in an inert atmosphere. Pt pans were used sample holders, whereas alumina powder was used as a reference material. The particle size and morphology of the synthesized material was analyzed through a transmission electron microscope (JEOL JEM-1200 EX II, Japan) by using 60−70 kV accelerating voltage.

2.2. Synthesis of 3-Oxo-3-phenyl-2-(2-phenylhydrazono)propanal-Based Ligands. *2.2.1. Synthesis of 3-(4-Chlorophenyl)-2-[2-(4-nitrophenyl)-hydrazono]-3-oxopropanal (4A).* 3-(4-Chlorophenyl)-2-[2-(4-nitrophenyl)hydrazono]-3-oxopropanal (**4A**) was prepared by following the already reported literature.[27−29] Briefly, sodium nitrite solution was prepared by taking 1 g of sodium nitrite in 10 mL of H_2O and was added to a cold solution of 10 mmol arylamine prepared in 5 mL of hydrochloride solution and continuously stirred for 30 min. The obtained solution of aryldiazonium was added to a cold solution of enaminone into 50 mL of ethanol containing sodium acetate (1 g in 10 mL H_2O). Then, the obtained mixture was continuously stirred for 1 h at room temperature. The required product was obtained by filtration and crystallized with water and ethanol. The whole

https://doi.org/10.1021/acsomega.3c01646
ACS Omega 2023, 8, 23633−23642

Scheme 1. Schematic Diagram Showing the Synthesis of the Ligands and Silver Complexes

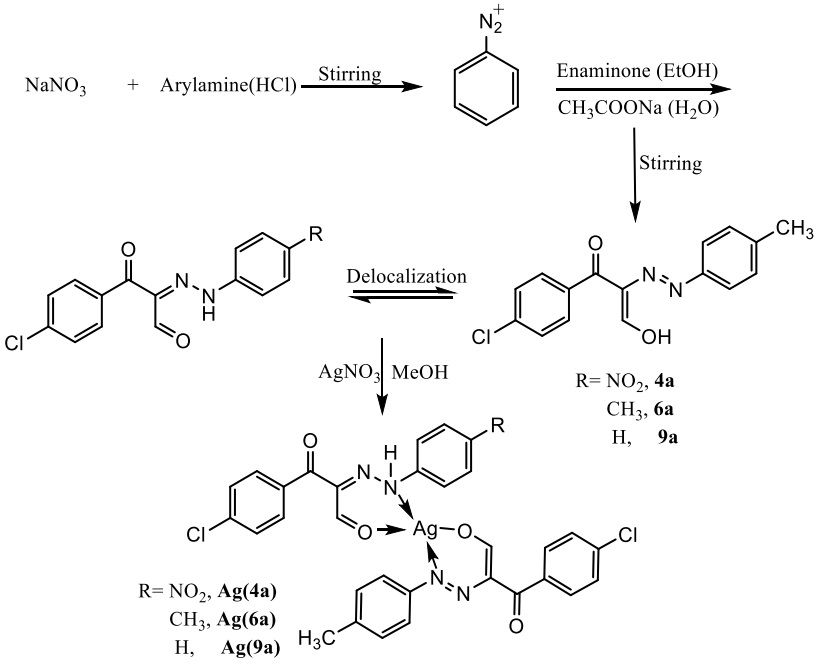

process resulted in the formation of yellow crystals of **4A** and in accordance with the reported literature;[30,31] yield 85%, mp 199 °C, IR ν_{max} cm^{-1}: 3114 (NH), 2952 (CH aldehyde), 1645 (C═O ester), 1592 (C═O aldehyde), 1514 (C═N). ^{1}HNMR: δ = 7.20−8.13 (m, 4H, Ar−H), 7.51−7.87 (m, 4H, Ar−H), 9.68 (S, 1H, CHO), 13.84 (s, 1H, NH) ppm (Figure S1A,B).

*2.2.2. Synthesis of 3-(4-Chlorophenyl)-2-[2-(4-methylphenyl)hydrazono]-3-oxopropanal (**6A**).* 3-(4-Chlorophenyl)-2-[2-(4-methylphenyl)hydrazono]-3-oxopropanal (**6A**) was prepared by using the same method as discussed for **4A**. Herein, we obtained dark yellow crystals of **6A** (Scheme 1), which is in line with previously reported data;[30,31] yield 90% mp 134 °C, IR ν_{max} cm^{-1}: 3057 (NH), 2845 (CH aldehyde), 1634 (C═O ester), 1587 (C═O aldehyde), 1528 (C═N). ^{1}HNMR: δ = 2.54 (s, 3H, CH_3), 7.45−7.50 (m, 4H, Ar−H), 7.51−7.87 (m, 4H, Ar−H), 9.68 (s, 1H, CHO), 13.24 (S, 1H, NH) ppm (Figure S2).

*2.2.3. Synthesis of 3-(4-Chlorophenyl)-3-oxo-2-(2-phenylhydrazono)propanal (**9A**).* 3-(4-Chlorophenyl)-3-oxo-2-(2-phenylhydrazono)propanal (**9A**) was also prepared similar to **4A**, thus resulting in the formation of yellow crystals[30,31] of **9A** (Scheme 1); yield 89% mp 136 °C, IR ν_{max} cm^{-1}: 3130 (NH), 2863 (CH aldehyde), 1633(C═O ester), 1591 (C═O aldehyde), 1516 (C═N). ^{1}HNMR: δ = 6.34−7.06 (m, 5H, Ar−H), 7.51−7.86 (m, 4H, Ar−H), 9.69 (s, 1H, CHO), 13.24 (s, 1H, NH) ppm (Figure S3A,B).

2.3. Synthesis of Ag(I) Complexes of Hydrazono oxi-Propanal Di-phenyl-Based Ligands. *2.3.1. Synthesis of Ag(**4A**).* An desired amount of 3-(4-chlorophenyl)-2-[2-(4-nitrophenyl)hydrazono]-3-oxopropanal (2 mmol in 20 mL methanol) was added to a solution of Ag(I) nitrate (2 mmol in 20 mL methanol). The resulting mixture was then refluxed and continuously stirred for 1 h. The obtained colored product was isolated by filtration, washed with hot methanol solution (Scheme 1), and dried under vacuum. Yellow crystals of Ag(**4A**) were obtained; yield 76% mp ≥ 300 °C, IR ν_{max} cm^{-1}: 3113 (NH), 2925 (broad CH aldehyde), 1644 (C═O ester), 1586 (C═O aldehyde), 1515 (C═N). ^{1}HNMR: δ = 6.16−6.95 (m, 8H, Ar−H), 7.28−8.62 (m, 8H, Ar−H), 9.01 (s, 2H, CHO), 13.05 (s, 1H, NH).

*2.3.2. Synthesis of Ag(**6A**).* A solution of 3-(4-chlorophenyl)-2-[2-(4-methylphenyl)hydrazono]-3-oxopropanal (2 mmol in 20 mL methanol) was added to a solution of Ag(I) nitrate (2 mmol in 20 mL methanol). The resulting mixture was refluxed and continuously stirred for 1 h. The obtained colored product was isolated by filtration, washed with hot methanol solution, and dried under vacuum. The resultant product of Ag(**6A**) were reddish yellow crystals; yield 81% mp ≥ 300 °C, IR ν_{max} cm^{-1}: 3114 (NH), 2880 (CH aldehyde), 1634 (C═O ester), 1587 (C═O aldehyde), 1529 (C═N). ^{1}HNMR: δ = 2.45 (s, 6H, CH_3), 6.28−6.41 (m, 8H, Ar−H), 6.65−6.95 (m, 8H, Ar−H), 9.03 (S, 2H, CHO), 13.38 (s, 1H, NH) ppm.

*2.3.3. Synthesis of Ag(**9A**).* A solution of 3-(4-chlorophenyl)-3-oxo-2-(2-phenylhydrazono)propanal (2 mmol in 20 mL methanol) was added to a solution of Ag(I) nitrate (2 mmol in 20 mL methanol). The resulting mixture was refluxed with stirring for 1 h. The obtained colored product (Scheme 1) was isolated by filtration, washed with hot methanol solution, and dried under vacuum. Reddish yellow crystals of Ag(**9A**) were obtained; yield 82% mp ≥ 300 °C, IR ν_{max} cm^{-1}: 3100 (NH), 2863 (CH aldehyde), 1634(C═O ester), 1591 (C═O aldehyde), 1516 (C═N). ^{1}HNMR: δ = 7.14−7.46 (m, 10H, Ar−H), 7.51−7.90 (m, 8H, Ar−H), 9.99 (s, 2H, CHO), 12.35 (s, 1H, NH) ppm.

2.4. DFT Calculations and Molecular Modeling. Density functional theory (DFT) was applied on **4A** and Ag(**4A**) samples. All were performed on the Gaussian06 package using the B3LYP/TD-FC basis set [25] and LANL2DZ [26].

2.5. Antimicrobial Assay. The antimicrobial efficacy of the synthesized Ag complexes was evaluated by using the already reported agar well diffusion strategy.[32,33] Briefly, *in vitro* antibacterial activity was assessed against both Gram-positive (*S. mutans* and *S. aureus*) and Gram-negative (*P. aeruginosa*, *E. coli*, and *klebsiella*) bacteria by using a nutrient

https://doi.org/10.1021/acsomega.3c01646
ACS Omega 2023, 8, 23633−23642

agar medium. Ampicillin and gentamicin were used as standard drugs against Gram-positive and Gram-negative bacteria. DMSO was used as a solvent control, whereas 15 mg/mL concentration of the synthesized Ag complexes was tested against both fungal and bacterial strains.

2.6. Method of Antimicrobial Testing. Antimicrobial testing was performed by using the already reported strategy.[34] Briefly, 20−25 mL of sterilized media was poured onto the Petri dishes (sterilized) and kept until solidified at room temperature. Sterilized saline equivalent to McFarland 0.5 standard solution (1.5×10^5 cfu mL^{-1}) was used to prepare the microbial suspension, and its turbidity was maintained by using a spectrophotometer (625 nm) to OD = 0.13. Once the turbidity of the inoculum suspension was adjusted, a sterile cotton swab was dipped to the maintained inoculum suspension, flooded on the dried agar surface, and allowed to dry for 15 min. Next, a sterile borer was used to dig wells of 6 mm diameter in the already solidified media. In the next step, 100 μL solution of the tested compound was filled in each well using a micropipette and incubated at room temperature (37 °C) for 24 h for the bacterial species, whereas the incubation period for the fungal species is 48 h. The experiment was conducted in triplicate, and zones of inhibition were measured (in the millimeter scale) to check the antibacterial activity.

3. RESULTS AND DISCUSSION

3.1. Compositional and Morphological Analysis of 4A, 6A, and 9A Ligands and Their Ag(I) Complexes. FTIR analysis was used to confirm the functional groups in the ligand and the synthesized complex (Figure 1). FTIR spectra

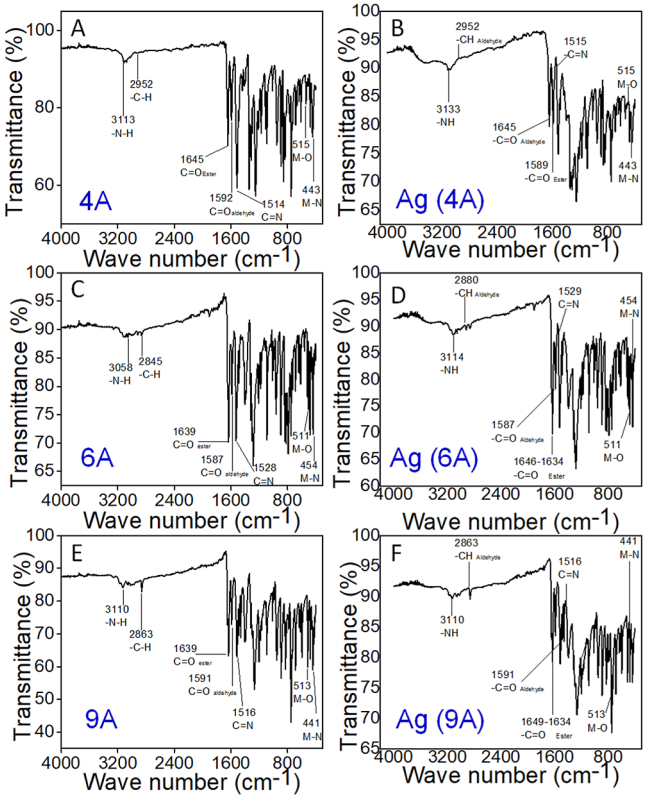

Figure 1. FTIR spectrum of free ligands (A) **4A**, (C) **6A**, and (E) **9A** and their respective Ag-coordinated complexes (B) Ag(**4A**), (D) Ag(**6A**), and (F) Ag(**9A**).

with bands depicting various functional groups, including −NH, −CH aldehyde, C═O ester, C═O aldehyde, and C═N, are shown in Table 1. It also indicates the presence of Ag−O and Ag−N bands in the case of complexes, confirming the successful formation of complexes and in accordance with the reported literature.[35] Briefly, the absorption band characteristics of C═N stretching modes were observed at 1514, 1528, and 1516 cm^{-1} for free ligands **4A**, **6A**, and **9A**, respectively (Figure 1A−C). Similarly, all these bands were also evident in the case of complexes, however with an insignificant positive frequency shift in the case of **4A** and **6A**. Additionally, aldehyde (C═O) symmetric vibrations for **4A**, **6A**, and **9A** were observed at 1592, 1587, and 1591 cm^{-1}, respectively. However, a shift toward lower frequency, *i.e.*, 1589 cm^{-1}, upon coordination with Ag was also observed in the case of **4A**, whereas no shift was evidenced in the case of both **6A** and **9A** complexes (Figure 1 and Table 1). The characteristic shift toward a lower frequency of C−H aldehyde stretching was observed in the case of **4A** complex, whereas a positive shift was detected in the **6A** complex. No shift in the peak frequency of C−H aldehyde stretching was detected in the **9A** complex.

3.2. Optical Properties. *3.2.1. Absorbance and Absorption Coefficient.* The synthesized ligands and their complexes with Ag(I) were further characterized through UV−visible spectroscopy to determine their stability and validity in optoelectronic applications. Results (Figure 2) reveal that both ligands **6A** and **9A** show spectral signaling at around λ_{max} 386 and 380 nm, respectively, because of in-plane quadrupole excitation. However, **4A** shows double absorption peaks with spectral signaling at around λ_{max} 393 and 520 nm, corresponding to in-plane quadrupole and dipolar excitation, respectively.[36] The increased absorption at 520 nm further reveals the presence of more in-plane dipolar excitation, and these results are in accordance with the reported literature.[37] The UV−visible spectra of Ag(I) complexes with these ligands (**4A**, **6A**, and **9A**) display similar spectral signaling at the same wavelength; however, a decrease in intensity is observed due to aggregation. For optoelectronic applications, the Ag-based ligand exhibits high absorbance, which leads to high absorption coefficient; hence, this synthesized Ag-based ligand can be viewed as a promising optoelectronic material, for example, organic solar cells and organic didoes.

3.2.2. Evolution of Band Gap and Urbach Energy for Optoelectronic Application. The major parameters that decide the validity of the material in optoelectronic applications like solar cells and organic didoes include absorption coefficient (proportional to absorbance = 2.303 × absorbance), optical band gap, and extended defects in the depletion region known as Urbach Energy.[38] The absorption process can be viewed as an electron moving from a lower to a higher energy state by absorbing a photon of known energy. Fundamental absorption is connected to band-to-band transition where a sudden rise known as the absorption edge can be used for the estimation of band gap of the synthesized compounds by Tauc's relations (eq 1).[39,40]

$$\alpha h\nu = A(h\nu - E_g)^m \quad (1)$$

Here, ν denotes the frequency, h is Planck's constant, E_g is the optical band gap, A is constantly relying on the effective masses associated with the band, and m is the complex parameter having the values m = 2, 1/2, 1/3, and 2/3.[41] In this work, m is found to be 1/2 that relates the direct transition occurred at zero wave factor (k = 0). The spectral dependence of $(\alpha h\nu)^2$

https://doi.org/10.1021/acsomega.3c01646
ACS Omega 2023, 8, 23633−23642

Table 1. Infrared Assignments of the Ligands and Their Ag Complexes

compounds	(NH)	(CH aliphatic)	(C=O ester)	(C=O aldehyde)	(C=N)	Ag−O	Ag−N
free ligand (**4A**)	3113	2952	1645	1592	1514		
Ag(**4A**)	3113	2925	1645	1589	1515	515	443
free ligand (**6A**)	3058	2845	1645−1634	1587	1528		
Ag(**6A**)	3114	2880	1646−1634	1587	1529	511	454
free ligand (**9A**)	3130	2863	1651−1633	1591	1516		
Ag(**9A**)	3110	2863	1649−1634	1591	1516	513	441

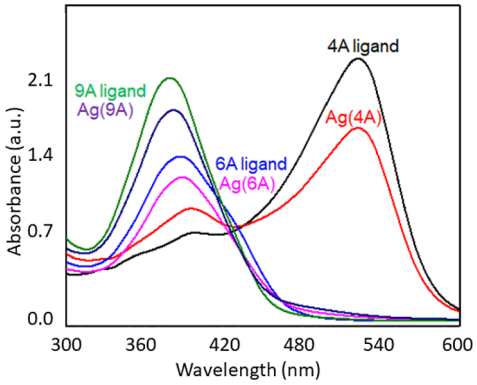

Figure 2. UV−vis spectrum of free ligands **4A**, **6A**, and **9A** and their respective Ag-coordinated complexes Ag(**4A**), Ag(**6A**), and Ag(**9A**).

on the incident energy is shown in Figure 3a−f for **4A**, **6A**, and **9A** and their respective Ag-coordinated complexes (Ag(**4A**), Ag(**6A**), and Ag(**9A**)). From these figures, the direct band gap can be precisely determined by applying graphical extrapolation of the best linear portion to the energy axis. Figure 3g represents the band gap values of different synthesized compounds. It is conspicuous that the band gap has higher values for **4A**, **6A**, and **9A** compared to their Ag-coordinated complexes. Therefore, we can conclude that the complex with Ag narrows the band gap which can be attributed to the change of the LUMO and HOMO positions because of the interference of d-orbital of Ag. Also, metals like Ag consider a zero band gap, thereby reducing the band gap when complexed with legends. It has been further observed that the band gap ranged from 2.18 to 2.90 eV, thus indicating the semiconductor nature of these complexes. Additionally, the Ag complexes have a bad gap that lies in the vision region of the solar spectrum, which reflects that Ag enhances the optical properties of ligands. Compared to pure ligands, Ag complexes can work effectively on dye-sensitized solar cells (DSSCs) and photodiodes as well as on visibly driven photocatalysts. A further reason that stands behind the band gap energies with Ag complexes is that Ag introduced localized states inside the space charge region which narrow the band gap. The Urbach energy is the term that determines the width of the localized states inside the band gap, which is connected to the absorption coefficient *via* the below relations (eq 2)[42,43]

$$\alpha = \alpha_o \exp(h\nu/E_u) \quad (2)$$

where α_o implies a characteristic parameter of the material, $h\nu$ refers to incident photon energy, and E_u is the Urbach energy which measures the band tail width of the localized states in the optical energy gap.[44] The values of E_u were computed by plotting the relation between ln (α) against $h\nu$. The slope of this relation can give directly the Urbach energy. A representation of Urbach energy of the different complexes is manifested in Figure 3h. By deep inspection of the figure, it can be observed that the trend of band gap energy is opposite to Urbach energy. This can be explained as the higher values of Urbach energy being partly responsible for lowering the band gap.

3.3. Thermogravimetric Analysis. The thermal stability of silver complexes (*i.e.*, **4A**, **6A**, and **9A**) was studied through simultaneous TGA and differential thermogravimetric (DTG) analysis. Thermal decomposition of Ag(**4A**) occurred in five successive decomposition steps ranging from 100 to 600 °C (Figure S4A). In the first step, it loses the coordinated water molecules in the lattice up to 200 °C with a mass loss of 19.45%.[45] The loss of water is an exothermal process, as evidenced by the DTG peak. Additionally, the presence of broad and intense peaks further confirms massive dehydration. The second step ranging from 201 to 390 °C represents the release of carbon monoxide and decomposition of organic moieties with an estimated mass loss of 25.91%. The third decomposition step is observed between 391 and 450 °C with a weight loss of 4.69%, corresponding to the loss of the rest of organic moieties. Similarly, the estimated mass loss occurring in the fourth and fifth decomposition step is around 6.05 and 5.08%, respectively, indicating the decomposition of the remaining moieties.

TGA and DTG analysis of Ag(**6A**) shows four-step decomposition (Figure S4B). The complex's dehydration takes place in the first step between 100 and 190 °C with a mass loss of ∼14.76%. The dehydration accompanied by an exothermal effect is represented by the DTG curve. The second and third decomposition steps represent the mass loss of organic moieties and release of carbon monoxide with an estimated mass loss of ∼32.00 and ∼14.66%, respectively, between 191 and 260 and 260 and 320 °C. The broad and intense DTG curve further confirms these results. The fifth decomposition step is observed between 320 and 800 °C and shows the removal of the remaining ligand with a mass loss of ∼15.97%.

Similarly, Ag(**9A**) shows four steps of thermal decomposition (Figure S4C). In the first step, a mass loss of 25.08% occurred between 100 and 190 °C due to the loss of water molecules. This loss is also evident from the intense DTG curve. The second decomposition step shows the mass loss of ∼18.97% from 190 to 250 °C, and the third decomposition shows the mass loss of 10.76% from 250 to 300 °C, indicating the release of carbon monoxide and the organic ligand. The fourth step shows the remaining ligand's removal with an estimated mass loss of ∼13.88% at 800 °C.

3.4. Morphological Investigation by TEM. The morphology and size of the synthesized complexes are evaluated through TEM images (Figure 4). The results indicate the clear and homogeneous formation of spherical shape nanoparticles with a size below 5 nm for all the three complexes. However, the average size of **9A** is observed to be

https://doi.org/10.1021/acsomega.3c01646
ACS Omega 2023, 8, 23633−23642

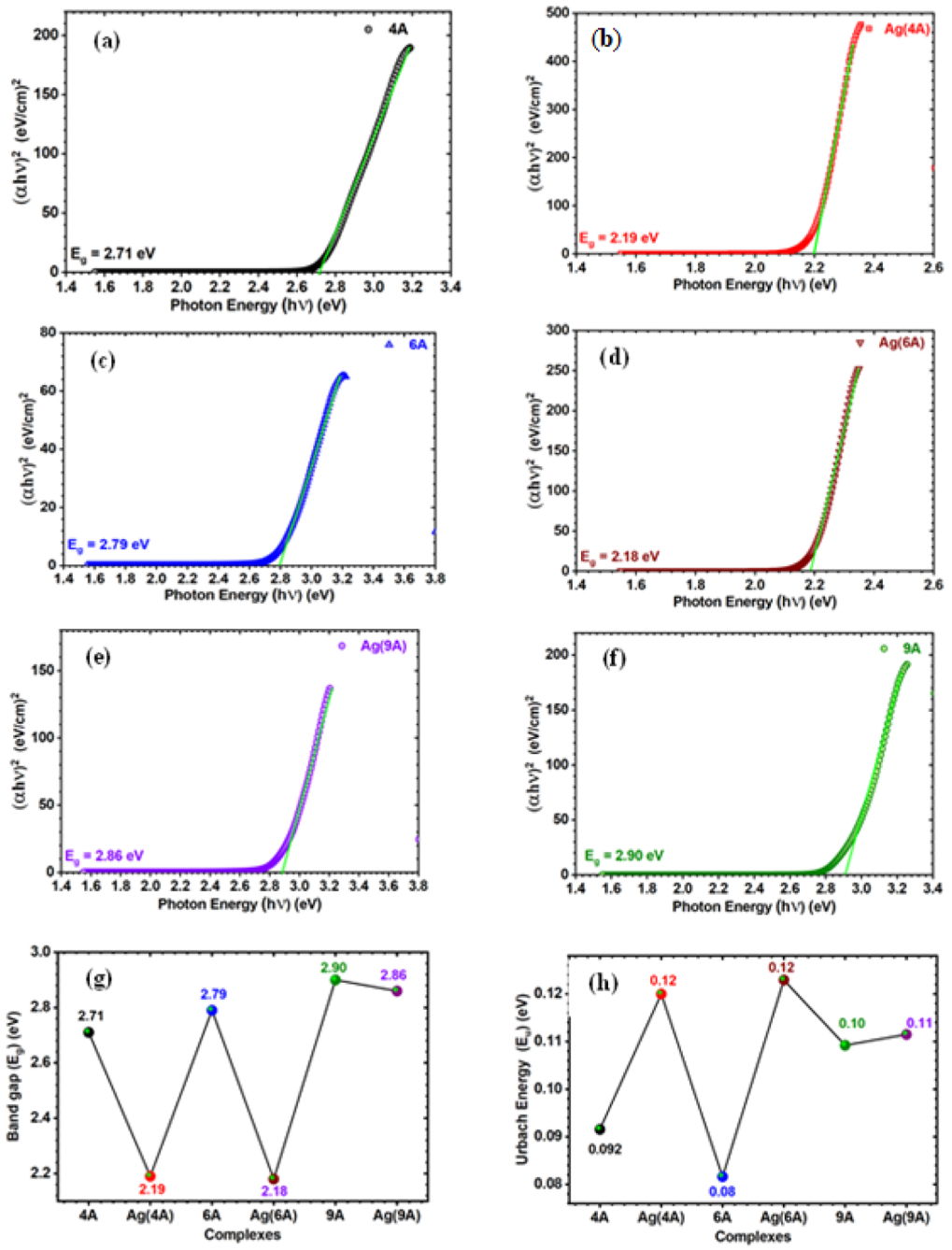

Figure 3. (a−f) Variation of $(\alpha h\nu)2$ and photon energy $(h\nu)$ for determination of band gap and (g,h) variation of band gap and Urbach energy for **4A**, **6A**, and **9A** and their respective Ag-coordinated complexes (Ag(**4A**), Ag(**6A**), and Ag(**9A**)).

much lower (∼2.05) compared to that of **6A** (∼2.5) and **4A** (∼2.8), respectively, and this could be attributed to the absence of bulky groups. The size of complexes is confirmed through zeta size analysis, and the results are in good agreement with TEM results.

3.5. DFT Calculations for 4A and Ag(4A). Molecules **4A** and Ag(**4A**) were optimized to explore the electronic geometric characteristics that may monitor their electron donation. The results show that the molecules are not planar, and NO_2 and Cl groups are oriented away from the central point (Figure 5). The structures of both possible arrangements are found to be stabilized through the hydrogen bonding formed between the hydroxyl and imino groups between the keto and amine groups. The bond length of the hydrogen bond in the keto-amine is shorter than the enol-imine form, thus indicating more stability of the enol-amine form. This supports the formation of the Ag(**4A**) complex (Scheme 1). The dipole/dipole of the amine form is 10.9826 kcal/mol, and the total energy is 38.6217 kcal/mol, whereas, for the enol form, the dipole/dipole energy is 5.1806 kcal/mol, and the total energy is 46.1611 kcal/mol. The HOMO−LUMO orbital occupation with the calculated energy gap for **4A** is shown in Figure 6.

3.6. Antimicrobial Efficacy of Ag(4A), Ag(6A), and Ag(9A) toward Drug-Resistant Pathogens. The antimicrobial activity was performed using the Agar well diffusion assay strategy,[32] and the results are shown in (Figure 7). The antimicrobial activity of these complexes was measured based

https://doi.org/10.1021/acsomega.3c01646
ACS Omega 2023, 8, 23633−23642

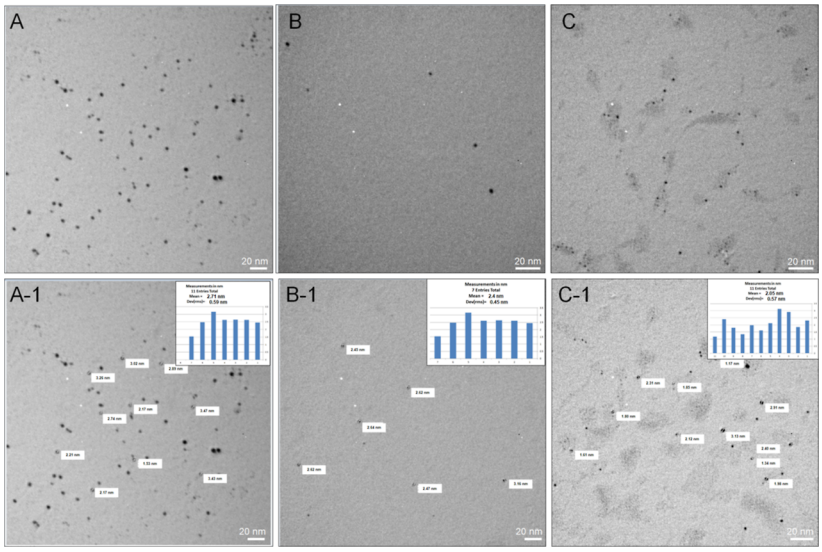

Figure 4. TEM images of Ag-coordinated complexes **4A** (A and A-1), **6A** (B and B-1), and **9A** (C and C-1) show the clear and homogeneous formation of nanoparticles. The inset shows the zeta size analysis of these complexes.

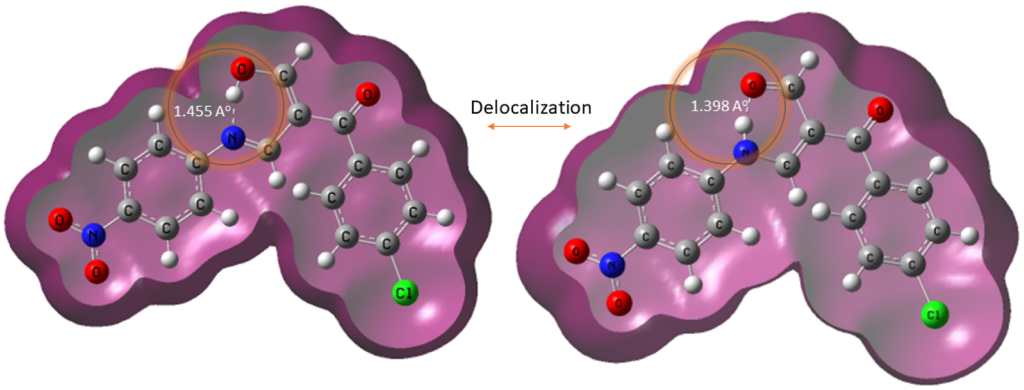

Figure 5. Optimized structures of **4A** with the possible formation of the keto-amine/enol-imine system. Hydrogen bonds are also displayed.

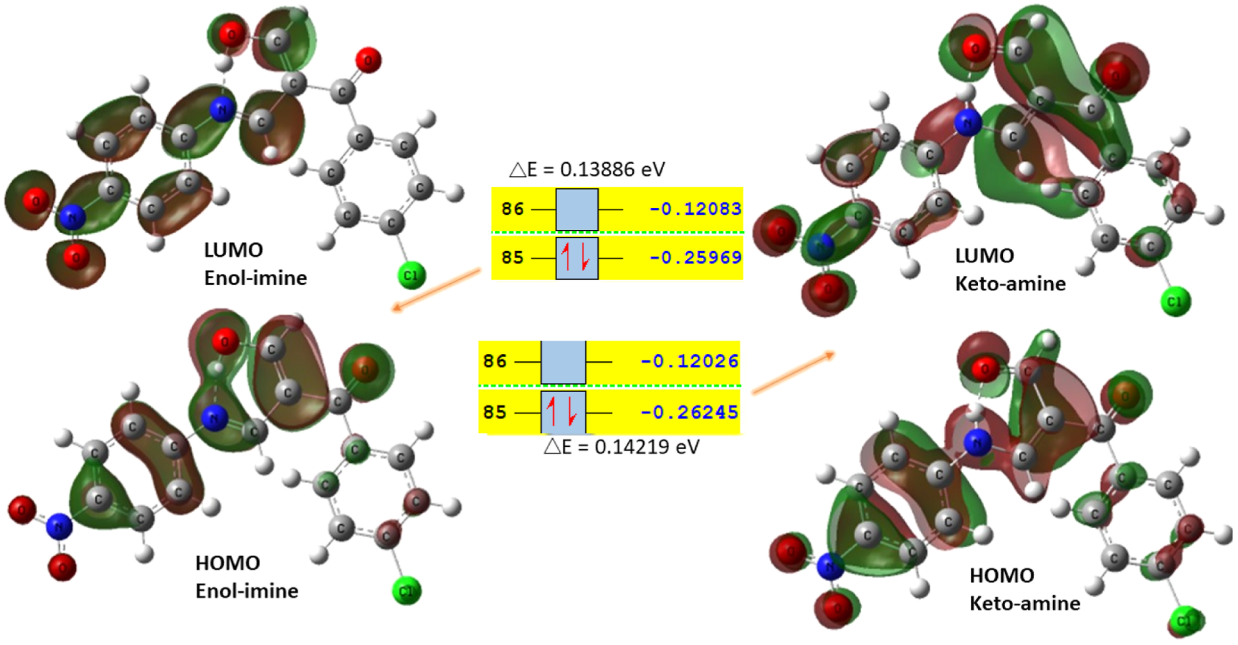

Figure 6. Optimized structures of **4A** (keto and enol forms) displaying the HOMO−LUMO orbital occupation with the calculated energy gap.

https://doi.org/10.1021/acsomega.3c01646
ACS Omega 2023, 8, 23633−23642

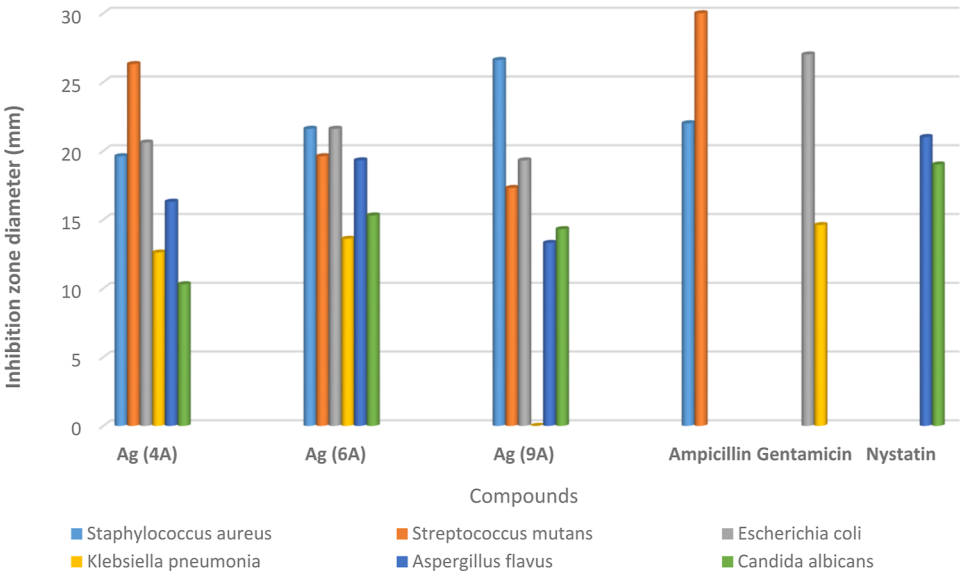

Figure 7. Antimicrobial activity of Ag complexes against various pathogens.

Table 2. Antimicrobial Activity of Ag Complexes (Ag(4A), Ag(6A), and Ag(9A)) against Various Pathogens[a]

	inhibition zone diameter (mm)					
	bacterial species					
	(Gm +ve)		(Gm −ve)		fungi	
compound	*S. aureus*	*S. mutans*	*E. coli*	*K. pneumonia*	*A. flavus*	*C. albicans*
DMSO	0.0	0.0	0.0	0.0	0.0	0.0
gentamicin			27 ± 0.5	14.6 ± 0.5		
ampicillin	22 ± 0.1	30 ± 0.5				
nystatin					21 ± 0.5	19 ± 0.5
Ag(**4A**)	19.6 ± 0.5	26.3 ± 0.6	20.6 ± 0.6	12.6 ± 0.5	16.3 ± 0.5	10.3 ± 0.5
Ag(**6A**)	21.6 ± 0.6	19.6 ± 0.6	21.6 ± 0.6	13.6 ± 0.6	19.3 ± 0.5	15.3 ± 0.5
Ag(**9A**)	26.6 ± 0.6	17.3 ± 0.6	19.3 ± 0.6	no activity	13.3 ± 0.5	14.3 ± 0.5

[a]Zone of inhibition (zoi) is expressed in the form of mean ± standard deviation (mm). NA: no activity, well diameter (6 mm), 100 μL of each sample was tested.

on the zone of inhibition (zoi) parameter, as shown in Table 2. It is interesting to mention that the Gram-negative bacteria *E. coli* was sensitive (based on zoi value) to all the three complexes, including Ag(**4A**), Ag(**6A**), and Ag(**9A**); however, Ag(**6A**) shows higher antimicrobial activity (zoi = 21.6 ± 0.6) and was much closer to standard antibiotic gentamicin (zoi = 27 ± 0.5).

In the case of *K. pneumonia*, the Ag complexes of **4A** and **6A** were observed to be very effective with zoi values 12.6 ± 0.5 and 13.6 ± 0.6, respectively. The observed value is very close to the standard antibiotic Gentamicin value 14.6 ± 0.5, confirming the efficient antibacterial activity of the novel complexes Ag(**4A**) and Ag(**6A**) toward *K. pneumonia*. In contrast, Ag(**9A**) shows no antibacterial activity against Gram-negative *K. pneumonia*.

The antimicrobial activity of Ag(**4A**), Ag(**6A**), and Ag(**9A**) against Gram-positive bacteria *S. aureus* was observed to be very efficient. Briefly, the antimicrobial activity of Ag(**9A**) was observed to be much higher (zoi = 26.6 ± 0.6) even compared to that of the standard antibiotic drug ampicillin (zoi = 22 ± 0.2), as shown in Table 2. The zoi value of Ag(**4A**) and Ag(**6A**) was observed to be very close to the ampicillin drug activity. On the other hand, the Ag complex with ligand **4A** shows a significant zoi value (26.3 ± 0.6) compared to **6A** (19.6 ± 0.6) and **9A** (17.3 ± 0.6) against *S. mutants*. Thus, Ag(**4A**) is effective against Gram-positive *S. mutants* and in good competition with the standard ampicillin (zoi = 30 ± 0.5).

Interestingly, all the synthesized complexes Ag(**4A**), Ag(**6A**), and Ag(**9A**) were observed to be active against fungi such as *C. albicans* and *Aspergillus flavus*. Ag(**6A**) exhibited the highest activity [(zoi = 19.3 ± 0.5) and (zoi = 15.3 ± 0.5)] against *A. flavus* and *C. albicans*, respectively. However, Ag(**9A**) (zoi = 13.3 ± 0.5) against *A. flavus* and Ag(**4A**) (zoi = 10.3 ± 0.5) against *C. albicans* displayed the lowest activities. These results suggest that the antimicrobial activity of novel Ag complexes (Ag(**4A**), Ag(**6A**), and Ag(**9A**)) against drug-resistant pathogens was found to be efficient.

4. CONCLUSIONS

Here, we reported the synthesis of novel Ag(I) complexes with 3-oxo-3-phenyl-2-(2-phenylhydrazono)propanal-based ligands to address the issue of antimicrobial resistance. The composition of the synthesized complexes were confirmed through FTIR and ^{1}H NMR, whereas morphological features and thermal stability were confirmed through TEM and TG/DTA analysis, respectively. Additionally, DFT studies further support the assumption that the enol form was reacted with

https://doi.org/10.1021/acsomega.3c01646
ACS Omega 2023, 8, 23633−23642

silver salts to give the silver complex. Interestingly, the results reveal that the synthesized complexes (Ag(**4A**), Ag(**6A**), and Ag(**9A**)) exhibit extraordinary antibacterial activity against a variety of drug-resistant pathogens including Gram-negative bacteria, Gram-positive bacteria, and fungi, thus possessing the enormous potential to act as an alternative to the conventionally employed drugs. Moreover, the synthesized complexes demonstrated the narrowing in the band gap, thus fulfilling the requirements for solar spectrum. Therefore, the complexation of Ag is very interesting for the functionalization of these compounds in DSSCs, organic photodiodes, and photocatalysis.

■ ASSOCIATED CONTENT

Supporting Information

The Supporting Information is available free of charge at https://pubs.acs.org/doi/10.1021/acsomega.3c01646.

^{1}H NMR, ^{13}C NMR, TGA, and DTG analysis (PDF)

■ AUTHOR INFORMATION

Corresponding Authors

Ahlam I. Al-Sulami − *College of Science, Department of Chemistry, University of Jeddah, Jeddah 21589, Saudi Arabia;* orcid.org/0000-0001-7844-2675; Email: 04102237@uj.edu.sa

Musa A. Said − *Chemistry Department, College of Science, Taibah University, Al-Madinah Al Munawara 1417, Saudi Arabia;* Present Address: Lehrstuhl fuer Anorganische Koordinationschemie Institut fuer Anorganische Chemie, University of Stuttgart, Pfaffenwaldring 55, 70569, Stuttgart, Germany; Email: masaid@taibahu.edu.sa

Authors

Maram T. Basha − *College of Science, Department of Chemistry, University of Jeddah, Jeddah 21589, Saudi Arabia;* orcid.org/0000-0002-1416-0844

Huda A. AlGhamdi − *College of Science, Department of Chemistry, University of Jeddah, Jeddah 21589, Saudi Arabia*

Sarah S. Albalawi − *College of Science, Department of Chemistry, University of Jeddah, Jeddah 21589, Saudi Arabia*

Khadijah M. Al-Zaydi − *College of Science, Department of Chemistry, University of Jeddah, Jeddah 21589, Saudi Arabia*

Complete contact information is available at: https://pubs.acs.org/10.1021/acsomega.3c01646

Notes

The authors declare no competing financial interest.

■ ACKNOWLEDGMENTS

This work was funded by the University of Jeddah, Saudi Arabia, under grant no. UJ-02-080-DR. Therefore, the authors acknowledge the University for technical and financial support.

■ REFERENCES

(1) Dhingra, S.; Rahman, N. A. A.; Peile, E.; Rahman, M.; Sartelli, M.; Hassali, M. A.; Islam, T.; Islam, S.; Haque, M. Microbial resistance movements: an overview of global public health threats posed by antimicrobial resistance, and how best to counter. *Front. Public Health* **2020**, *8*, 535668.

(2) Ting, D. S. J.; Ho, C. S.; Deshmukh, R.; Said, D. G.; Dua, H. S. Infectious keratitis: an update on epidemiology, causative microorganisms, risk factors, and antimicrobial resistance. *Eye* **2021**, *35*, 1084−1101.

(3) Cassir, N.; Rolain, J.-M.; Brouqui, P. A new strategy to fight antimicrobial resistance: the revival of old antibiotics. *Front. Microbiol.* **2014**, *5*, 551.

(4) (a) Santajit, S.; Indrawattana, N. Mechanisms of antimicrobial resistance in ESKAPE pathogens. *BioMed Res. Int.* **2016**, *2016*, 2475067. (b) Ramsamy, Y.; Essack, S. Y.; Sartorius, B.; Patel, M.; Mlisana, K. P. Antibiotic resistance trends of ESKAPE pathogens in Kwazulu-Natal, South Africa: a five-year retrospective analysis. *Afr. J. Lab. Med.* **2018**, *7*, 887.

(5) El-Gammal, O. A.; El-Bindary, A. A.; Sh Mohamed, F.; Rezk, G. N.; El-Bindary, M. A. Synthesis, characterization, design, molecular docking, anti COVID-19 activity, DFT calculations of novel Schiff base with some transition metal complexes. *J. Mol. Liq.* **2022**, *346*, 117850.

(6) Rüping, M. J.; Vehreschild, J. J.; Cornely, O. A. Patients at high risk of invasive fungal infections. *Drugs* **2008**, *68*, 1941−1962.

(7) Cabello, F. C.; Godfrey, H. P.; Tomova, A.; Ivanova, L.; Dölz, H.; Millanao, A.; Buschmann, A. H. Antimicrobial use in aquaculture re-examined: its relevance to antimicrobial resistance and to animal and human health. *Environ. Microbiol.* **2013**, *15*, 1917−1942.

(8) (a) Olaimat, A. N.; Al-Holy, M. A.; Shahbaz, H. M.; Al-Nabulsi, A. A.; Abu Ghoush, M. H.; Osaili, T. M.; Ayyash, M. M.; Holley, R. A. Emergence of antibiotic resistance in Listeria monocytogenes isolated from food products: a comprehensive review. *Compr. Rev. Food Sci. Food Saf.* **2018**, *17*, 1277−1292. (b) Gemmell, C. G.; Edwards, D. I.; Fraise, A. P.; Gould, F. K.; Ridgway, G. L.; Warren, R. E. Guidelines for the prophylaxis and treatment of methicillin-resistant Staphylococcus aureus (MRSA) infections in the UK. *J. Antimicrob. Chemother.* **2006**, *57*, 589−608.

(9) Gemmell, C. G.; Edwards, D. I.; Fraise, A. P.; Gould, F. K.; Ridgway, G. L.; Warren, R. E. Guidelines for the prophylaxis and treatment of methicillin-resistant Staphylococcus aureus (MRSA) infections in the UK. *J. Antimicrob. Chemother.* **2006**, *57*, 589−608.

(10) (a) Singh, S.; Mishra, P. Bacitracin and isothiocyanate functionalized silver nanoparticles for synergistic and broad spectrum antibacterial and antibiofilm activity with selective toxicity to bacteria over mammalian cells. *Biomater. Adv.* **2022**, *133*, 112649. (b) Shumbula, N. P.; Nkabinde, S. S.; Ndala, Z. B.; Mpelane, S.; Shumbula, M. P.; Mdluli, P. S.; Njengele-Tetyana, Z.; Tetyana, P.; Hlatshwayo, T.; Mlambo, M. Evaluating the antimicrobial activity and cytotoxicity of polydopamine capped silver and silver/polydopamine core-shell nanocomposites. *Arab. J. Chem.* **2022**, *15*, 103798.

(11) Shumbula, N. P.; Nkabinde, S. S.; Ndala, Z. B.; Mpelane, S.; Shumbula, M. P.; Mdluli, P. S.; Njengele-Tetyana, Z.; Tetyana, P.; Hlatshwayo, T.; Mlambo, M.; et al. Evaluating the antimicrobial activity and cytotoxicity of polydopamine capped silver and silver/polydopamine core-shell nanocomposites. *Arab. J. Chem.* **2022**, *15*, 103798.

(12) Djokić, S. Synthesis and Antimicrobial Activity of Silver Citrate Complexes. *Bioinorg. Chem. Appl.* **2008**, *2008*, 436458.

(13) Zhao, M.; Zhou, M.; Gao, P.; Zheng, X.; Yu, W.; Wang, Z.; Li, J.; Zhang, J. AgNPs/nGOx/Apra Nanocomposites for Synergistic Antimicrobial Therapy and Scarless Skin Recovery. *J. Mater. Chem. B* **2022**, *10*, 1393.

(14) Khina, A. G.; Krutyakov, Y. A. Similarities and Differences in the Mechanism of Antibacterial Action of Silver Ions and Nanoparticles. *Appl. Biochem. Microbiol.* **2021**, *57*, 683−693.

(15) Rajendran, R.; Pullani, S.; Thavamurugan, S.; Radhika, R.; Lakshmi Prabha, A. J. A. N. Green fabrication of silver nanoparticles from Salvia species extracts: characterization and anticancer activities against A549 human lung cancer cell line. *Appl. Nanosci.* **2022**, *13*, 2571.

(16) Patzke, G. R.; Zhou, Y.; Kontic, R.; Conrad, F. Oxide nanomaterials: synthetic developments, mechanistic studies, and technological innovations. *Angew. Chem., Int. Ed.* **2011**, *50*, 826−859.

(17) El-Bindary, M. A.; El-Bindary, A. A. Synthesis, characterization, DNA binding, and biological action of dimedone arylhydrazone chelates. *Appl. Organomet. Chem.* **2022**, *36*, No. e6576.

(18) Ahmad, S.; Hanif, M.; Monim-ul-Mehboob, M.; Isab, A. A.; Alotaibi, M. A.; Ahmad, T. J. P. Versatile coordination chemistry of mixed ligand silver (I) complexes of phosphanes and thioamides: structural features and biological properties. *Polyhedron* **2022**, *214*, 115643.
(19) Ahmed, Y. M.; Mohamed, G. G. Synthesis, Spectral Characterization, Antimicrobial Evaluation and Molecular docking studies on New Metal Complexes of Novel Schiff base derived from 4, 6-dihydroxy-1, 3-phenylenediethanone. *J. Mol. Struct.* **2022**, *1256*, 132496.
(20) Aquaroni, N. A. S.; Nakahata, D. H.; Lazarini, S. C.; Resende, F. A.; Cândido, A. L.; da Silva Barud, H.; Claro, A. M.; de Carvalho, J. E.; Ribeiro, C. M.; Pavan, F. R.; Pavan, F. R.; et al. Antibacterial activities and antiproliferative assays over a tumor cells panel of a silver complex with 4-aminobenzoic acid: Studies in vitro of sustained release using bacterial cellulose membranes as support. *J. Inorg. Biochem.* **2020**, *212*, 111247.
(21) Shoair, A.; El-Bindary, A.; El-Ghamaz, N.; Rezk, G. Synthesis, characterization, DNA binding and antitumor activities of Cu (II) complexes. *J. Mol. Liq.* **2018**, *269*, 619−638.
(22) Al-Hazmi, G. A.; Abou-Melha, K. S.; Althagafi, I.; El-Metwaly, N.; Shaaban, F.; Abdul Galil, M. S.; El-Bindary, A. A. Synthesis and structural characterization of oxovanadium (IV) complexes of dimedone derivatives. *Appl. Organomet. Chem.* **2020**, *34*, No. e5672.
(23) Kiwaan, H. A.; El-Mowafy, A. S.; El-Bindary, A. A. Synthesis, spectral characterization, DNA binding, catalytic and in vitro cytotoxicity of some metal complexes. *J. Mol. Liq.* **2021**, *326*, 115381.
(24) Wu, T.; Wang, L.; Zhao, R.; Zhuang, R.; Zhao, K.; Liu, G.; Huang, J.; Sun, L.; Hua, Y. Highly stable perovskite solar cells with a novel Ni-based metal organic complex as dopant-free hole-transporting material. *J. Energy Chem.* **2022**, *65*, 312−318.
(25) Xu, J.; Buin, A.; Ip, A. H.; Li, W.; Voznyy, O.; Comin, R.; Yuan, M.; Jeon, S.; Ning, Z.; McDowell, J. J.; et al. Perovskite-fullerene hybrid materials suppress hysteresis in planar diodes. *Nat. Commun.* **2015**, *6*, 7081.
(26) Scholar, P. *Antimicrobial and Wound Healing Activity of Jasminum Grandiflorum Linn: a Review*, 2019.
(27) Al-Awadi, N. A.; Elnagdi, M. H.; Ibrahim, Y. A.; Kaul, K.; Kumar, A. Efficient synthesis of 3-aroylcinnolines from aryl methyl ketones. *Tetrahedron* **2001**, *57*, 1609−1614.
(28) Al-Awadi, N. A.; Ibrahim, M. R.; Abdelhamid, I. A.; Elnagdi, M. H. Arylhydrazonals as the aldehyde component in Baylis−Hillman reactions. *Tetrahedron* **2008**, *64*, 8202−8205.
(29) Al-Omran, F.; Al-Awadi, N.; El-Khair, A. A.; Elnagdi, M. H. Synthesis of new aryl and heteroaromatic substituted pyridines, pyrazoles, pyrimidines and pyrazolo [3, 4-d] pyridazines. *Org. Prep. Proced. Int.* **1997**, *29*, 285−292.
(30) Al-Zaydi, K. M.; Borik, R. M.; Elnagdi, M. H. 2-Arylhydrazonopropanals as building blocks in heterocyclic chemistry: Microwave assisted condensation of 2-aryl-hydrazonopropanals with amines and active methylene reagents. *Molecules* **2003**, *8*, 910−923.
(31) Al-Zaydi, K. M.; Borik, R. M. Microwave assisted condensation reactions of 2-aryl hydrazonopropanals with nucleophilic reagents and dimethyl acetylenedicarboxylate. *Molecules* **2007**, *12*, 2061−2079.
(32) Gercek, Y. C.; Celik, S.; Bayram, S. Screening of Plant Pollen Sources, Polyphenolic Compounds, Fatty Acids and Antioxidant/Antimicrobial Activity from Bee Pollen. *Molecules* **2022**, *27*, 117.
(33) El-Bindary, M. A.; El-Desouky, M. G.; El-Bindary, A. A. Metal−organic frameworks encapsulated with an anticancer compound as drug delivery system: Synthesis, characterization, antioxidant, anticancer, antibacterial, and molecular docking investigation. *Appl. Organomet. Chem.* **2022**, *36*, No. e6660.
(34) Hassan, S. S.; Khalf-Alla, P. A. Anti-hepatocellular carcinoma, antioxidant, anti-inflammation and antimicrobial investigation of some novel first and second transition metal complexes. *Appl. Organomet. Chem.* **2020**, *34*, No. e5432.
(35) Dhand, V.; Soumya, L.; Bharadwaj, S.; Chakra, S.; Bhatt, D.; Sreedhar, B. Green synthesis of silver nanoparticles using Coffea arabica seed extract and its antibacterial activity. *Mater. Sci. Eng. C* **2016**, *58*, 36−43.
(36) Ghosh, S. K.; Pal, T. Interparticle coupling effect on the surface plasmon resonance of gold nanoparticles: from theory to applications. *Chem. Rev.* **2007**, *107*, 4797−4862.
(37) Waqas, M.; Zulfiqar, A.; Ahmad, H. B.; Akhtar, N.; Hussain, M.; Shafiq, Z.; Abbas, Y.; Mehmood, K.; Ajmal, M.; Yang, M. Fabrication of highly stable silver nanoparticles with shape-dependent electrochemical efficacy. *Electrochim. Acta* **2018**, *271*, 641−651.
(38) Chen, W.; Cao, W.; Hameed, T. A.; Marsillac, S.; Elsayed-Ali, H. E. Properties of Cu(In,Ga,Al)Se_2 thin films fabricated by pulsed laser deposition. *J. Mater. Sci.: Mater. Electron.* **2014**, *26*, 1743−1747.
(39) (a) Ghanem, M. G.; Badr, Y.; Hameed, T. A.; El Marssi, M.; Lahmar, A.; Wahab, H. A.; Battisha, I. K. Synthesis and characterization of undoped and Er-doped ZnO nano-structure thin films deposited by sol-gel spin coating technique. *Mater. Res. Express* **2019**, *6*, 085916. (b) Yousef, T. A.; Abu El-Reash, G. M.; El-Gammal, O. A.; Bedier, R. A. Synthesis, characterization, optical band gap, in vitro antimicrobial activity and DNA cleavage studies of some metal complexes of pyridyl thiosemicarbazone. *J. Mol. Struct.* **2013**, *1035*, 307−317.
(40) Yousef, T.; Abu El-Reash, G.; El-Gammal, O.; Bedier, R. Synthesis, characterization, optical band gap, in vitro antimicrobial activity and DNA cleavage studies of some metal complexes of pyridyl thiosemicarbazone. *J. Mol. Struct.* **2013**, *1035*, 307−317.
(41) Mohamed, F.; Sharmoukh, W.; Youssef, A. M.; Hameed, T. A. Structural, morphological, optical, and dielectric properties of PVA-PVP filled with zinc oxide aluminum-graphene oxide composite for promising applications. *Polym. Adv. Technol.* **2022**, *33*, 1009−1020.
(42) (a) Hameed, T. A.; Cao, W.; Mansour, B. A.; Elzawaway, I. K.; Abdelrazek, E.-M. M.; Elsayed-Ali, H. E. Properties of Cu(In,Ga,Al)-Se_2 thin films fabricated by magnetron sputtering. *J. Vac. Sci. Technol., A* **2015**, *33*, 031201. (b) Urbach, F. The Long-Wavelength Edge of Photographic Sensitivity and of the Electronic Absorption of Solids. *Phys. Rev.* **1953**, *92*, 1324.
(43) Urbach, F. The long-wavelength edge of photographic sensitivity and of the electronic absorption of solids. *Phys. Rev.* **1953**, *92*, 1324.
(44) Hameed, T. A.; Azab, A. A.; Ibrahim, R. S.; Rady, K. E. Optimization, structural, optical and magnetic properties of TiO2/CoFe2O4 nanocomposites. *Ceram. Int.* **2022**, *48*, 20418−20425.
(45) Zhang, L.-P.; Lam, C.-K.; Song, H.-B.; Mak, T. C. Crystalline hydrates and polymeric Ag (I) complexes of isomeric flexible double betaines 1, 4-bis (n-picolyloxyl) benzene-N, N′-diacetate (n= 2, 3, 4). *Polyhedron* **2004**, *23*, 2413−2425.

https://doi.org/10.1021/acsomega.3c01646
ACS Omega 2023, 8, 23633−23642